Original Article

Genetic and molecular insights into genotype-phenotype relationships in osteopathia striata with cranial sclerosis (OSCS) through the analysis of novel mouse *Wtx* mutant alleles[†]

Glenda Comai[1,9]*, Agnès Boutet[1,10], Kristina Tanneberger[2], Filippo Massa[1], Ana-Sofia Rocha[1], Aurelie Charlet[1], Clara Panzolini[1], Fariba Jian Motamedi[1], Robert Brommage[3], Wolfgang Hans[3], Thomas Funck-Brentano[7,8], Martin Hrabe de Angelis[3,4,5], Christine Hartmann[6], Martine Cohen-Solal[7,8], Jürgen Behrens[2] and Andreas Schedl[1]*

[1]Université Côte d'Azur, Inserm, CNRS, iBV, France
[2]Friedrich-Alexander Universität Erlangen-Nuremberg, Nikolaus Fiebiger Zentrum, 91054 Erlangen Germany
[3]German Mouse Clinic, Institute of Experimental Genetics, Helmholtz Zentrum München, German Research Center for Environmental Health, Ingolstädter Landstrasse 1, 85764 Neuherberg, Germany
[4]Chair of Experimental Genetics, School of Life Science Weihenstephan, Technische Universität München, Alte Akademie 8, 85354 Freising, Germany
[5]German Center for Diabetes Research (DZD), Ingolstädter Landstrasse 1, 85764 Neuherberg, Germany
[6]Institute of Musculoskeletal Medicine, University Hospital Münster, WWU, Domagkstrasse 3, 48149 Münster, Germany
[7]Inserm UMR-1132, BIOSCAR, Paris, France
[8]Université Paris Diderot, Sorbonne Paris Cité, Paris, France
[9]Current Address: Dept. of Developmental & Stem Cell Biology, Pasteur Institute, CNRS UMR3738, Paris, France
[10]Current Address: CNRS, Sorbonne Université, UPMC Univ Paris 6, UMR8227, Translation, Cell Cycle and Development Group, Station Biologique, F-29688 Roscoff, France

[†]This article has been accepted for publication and undergone full peer review but has not been through the copyediting, typesetting, pagination and proofreading process, which may lead to differences between this version and the Version of Record. Please cite this article as doi: [10.1002/jbmr.3387]

Additional Supporting Information may be found in the online version of this article.

Initial Date Submitted June 30, 2017; Date Revision Submitted December 19, 2017; Date Final Disposition Set January 3, 2018

Journal of Bone and Mineral Research

DOI 10.1002/jbmr.3387

* corresponding authors: Andreas Schedl
iBV, Institut de Biologie Valrose,
Univ. Nice Sophia Antipolis,
Centre de Biochimie; UFR Sciences;
Parc Valrose,
28, avenue Valrose,
06108 Nice Cedex 2, France
E-mail: schedl@unice.fr
Phone: +33 -0- 49207640

Glenda Comai
Institut Pasteur - CNRS UMR3738
25 Rue du Dr. Roux, 75015, Paris, FRANCE
E-mail: comai@pasteur.fr
Phone: +33 1 40 61 38 54

Conflict of interest statement: No conflicts declared

Abstract

The X-linked WTX/AMER1 protein forms an important component of the β-catenin destruction complex that can both enhance and suppress canonical β-catenin signalling. Somatic mutations in WTX/AMER1 have been found in a proportion of the pediatric kidney cancer Wilms' tumour. By contrast, germline mutations cause the severe sclerosing bone dysplasia osteopathia striata congenita with cranial sclerosis (OSCS), a condition usually associated with fetal or perinatal lethality in male patients. Here we addressed the developmental and molecular function of WTX by generating two novel mouse alleles. We show that in addition to the previously reported skeletal abnormalities, loss of *Wtx* causes severe midline fusion defects including cleft palate and ectopic synostosis at the base of the skull. By contrast, deletion of the C-terminal part of the protein results in only mild developmental abnormalities permitting survival beyond birth. Adult analysis however revealed skeletal defects including changed skull morphology and an increased whole body bone density, resembling a subgroup of male patients carrying a milder, survivable phenotype. Molecular analysis *in vitro* demonstrated that while β-catenin fails to co-immunoprecipitate with the truncated protein, partial recruitment appears to be achieved in an indirect manner using AXIN/AXIN2 as a molecular bridge. Taken together our analysis provides a novel model for WTX-caused bone diseases and explains on the molecular level how truncation mutations in this gene may retain some of WTX-protein functions.

Keywords: Bone development, β-catenin signalling, OSCS, mouse models

Introduction

β-catenin is a multifunctional protein that plays important roles in cellular adhesion and as a signal transducer in the canonical Wnt signalling pathway [1,2]. Under normal conditions, free β-catenin quickly associates with AXIN, APC and GSK3β in a multiprotein complex. Phosphorylation of β-catenin by GSK3β leads to its targeting to the proteasome pathway and its rapid degradation, thus keeping cytoplasmic β-catenin levels low. Binding of a WNT ligand to its receptors Frizzled (Fz) and the low-density lipoprotein receptor-related protein LRP5/6 results in recruitment of AXIN to the membrane and the disruption of the degradation complex. As a result, β-catenin is no longer phosphorylated, accumulates in the cell and translocates to the nucleus, where it interacts with DNA-binding proteins to regulate downstream effector genes [3]. Given its central role in the canonical Wnt signalling pathway, it is not surprising that loss-of-function mutations in β-catenin, or in one of its modulators, lead to serious developmental abnormalities in a wide variety of tissues [1]. Moreover, mutations that cause an increase in β-catenin levels are often associated with cancers [4] including the paediatric kidney cancer Wilms' tumour [5].

WTX/AMER1 is X-chromosome linked and has been identified as a gene carrying somatic mutations in a proportion of Wilms' tumours [6]. On a molecular level WTX appears to form part of the AXIN/APC/GSK3β multiprotein complex [7-9]. A series of experiments have demonstrated that WTX enhances β-catenin ubiquitination and degradation and therefore can act as a negative regulator of canonical WNT signalling [8,9]. In addition, molecular studies suggested that WTX also recruits GSK3β to the membrane, where it can stimulate LRP6 phosphorylation, at least *in vitro* [10]. Biochemical and cellular studies have revealed seven conserved residues in the N-terminus of WTX that are crucial for its binding to the plasma membrane [8] and four domains that confer binding to APC [7,11]. WTX also contains two regions capable of interacting with AXIN1/AXIN2 [8,10]. On the other hand the C-terminal half of this protein was shown to directly bind to β-catenin [8,9]. This C-terminal domain was also suggested to mediate translocation of the WTX protein to the nucleus, where it can interact with another Wilms' tumour suppressor protein, WT1, and stimulate its activity as a transcriptional regulator *in vitro* [12], and also act as a modulator of p53 function [13].

While somatic mutations in *WTX* are associated with Wilms' tumours, germline mutations in this gene do not trigger kidney tumours, but instead cause the X-linked dominant congenital skeletal disease osteopathia striata congenita with cranial sclerosis (OSCS; OMIM 300373) [14,15]. In heterozygous females, this condition is characterized by sclerosis of the long bones and skull, longitudinal striations visible on radiographs in the metaphyseal regions of the long bones, pelvis and scapulae. Other common clinical findings of OSCS include craniofacial malformations (macrocephaly, frontal bossing, ocular hypertelorism, a broad nasal bridge), hearing loss, abnormalities of the palate and mild learning difficulties [14-16]. Hemizygous mutations in males are typically associated with fetal or neonatal lethality due to an array of developmental malformations (i.e. omphalocele, limb patterning, genitourinary and cardiac defects) besides the sclerotic bone phenotype [14,17]. However, there are subgroups of male patients, which carry truncation mutations at or after the 2nd APC binding domain that cause a milder phenotype resembling those of heterozygous female patients and permit survival to adulthood [14,17]. The molecular explanation for these less severe phenotypes is unclear, but it has been speculated that these truncated proteins retain some functionality with the retention of the N-terminal WTX membrane interaction domain and at least one of the three APC binding sites [14].

The Wnt/β-catenin signalling pathway has been shown to play key roles in bone formation and bone homeostasis in the adult. Consequently, mutations that affect β-catenin expression levels and β-catenin activity often result in skeletal defects [18]. A role for WTX as a negative regulator of β-catenin stability fits therefore well with the observed bone malformations in OSCS patients. Indeed, deletion of *Wtx* in mice leads to tissue overgrowth, increased bone density and loss of adipose tissue [19]. On a molecular level this phenotype has been attributed to a role for WTX in controlling the switch of mesenchymal precursors between the adipocyte and osteoblast lineage through the regulation of β–catenin levels.

In the present study we further dissected the developmental and molecular function of WTX *in vivo* by generating a loss-of-function and a hypomorph allele in the mouse. Consistent with earlier observations, complete loss of *Wtx* causes perinatal death and we describe a range of previously unreported severe midline skeletal defects. Surprisingly, deletion of the C-terminal half of *Wtx* (*Wtx*$^{flox\Delta}$ allele) is compatible with postnatal life and results only in relatively minor developmental bone patterning defects. Our *in vitro* data revealed that the truncated WTX$^{flox\Delta}$ protein can localize to the plasma membrane, and interact with β-catenin and GSK3β indirectly through its association with the scaffolding proteins AXIN1/AXIN2. Compensation, however, is incomplete and adult mice display skeletal dysplasia that recapitulates the phenotype found in human XY patients with 3' deletions.

Materials and Methods

Mice

The targeting construct of the conditional *Wtx* allele was obtained by insertion of a first loxP into a ClaI site 337 bp upstream of the first ATG in exon2 and insertion of a floxed *PGK-Neomycin-HSV-thymidine kinase* cassette into a BamHI site 1674 bp downstream the first codon (Suppl. Figure 1.A.a). Screening for positively targeted R1 embryonic stem (ES) cells [20] after Neomycin selection was first performed by nested PCR with Targ_fw/pflox225/Targ_fw2 primers (Suppl. Figure 1.A.a). Positively targeted ES cells were confirmed by Southern blot using an external 3’ probe on PstI-digested genomic DNA (Suppl. Figure 1B). The PGK-NEO/HSVtk cassette was removed *in vitro* by electroporation of targeted ES cells with a Cre recombinase expression vector and FIAU selection (Suppl. Figure 1.A.b). Chimeric mice containing the $Wtx^{flox\Delta}$ allele were obtained by injection of $Wtx^{flox\Delta}$ ES cells into C57BL/6J mouse blastocysts. The Wtx^{KO} allele was obtained *in vivo* by germline deletion of the $Wtx^{flox\Delta}$ allele with the *Deleter Cre* [(21)] or *Sox2-Cre* [(22)] lines (Suppl. Figure 1.A.c). Routine genotyping was performed by PCR from earmarks or tail tips using the following primers: Primer_a: tggacgcaactcagagatgt and Primer_b: caactgcttctggatggtca for the flox allele, and Primer_c: ttggtcaggatggatgattg and Primer_b for the KO allele (Suppl. Figure 1.A.b, 1.A.c, Suppl. Figure 2.C). All genotyping PCR reactions were carried out in the GoTaq® Green Master Mix (Promega).

Control and mutant mice were analyzed as littermates on a 129xC57Bl/6 hybrid background. All animal work was conducted according to national and international guidelines and was approved by the local ethics committee (PEA-NCE/2013-88). Animals were bred following the scheme on Suppl. Figure 2A, B**.** The conditional *β-catenin* mouse line has been described previously [(23)]. Compound Wtx^{KO}*;* β*-catenin*$^{KO/+}$ embryos were generated by crossing *Deleter Cre+* or *Sox2-Cre+* β*-catenin*$^{fl/+}$males with $Wtx^{KO/+}$ female mice. To obtain embryos at the desired developmental stages, young adult $Wtx^{flox\Delta/+}$ or $Wtx^{KO/+}$ females were mated overnight, and animals with a vaginal plug at noon of the next day were considered as embryonic day (E) 0.5. Pregnant females were euthanized by cervical dislocation.

Plasmid constructions

The mouse *Wtx* expression plasmid (GFP-Wtx) has been described elsewhere [(24)]. The expression construct for the $Wtx^{flox\Delta}$ allele (GFP-$Wtx^{flox\Delta}$) was generated by insertion of the BstXI-ScaI restriction fragment, flanking the loxP site of the targeting construct, into the Wtx wildtype expression plasmid cut with the same enzymes. pcDNA-Flag-Axin1 has been provided by A. Kikuch. pcDNA-Flag-Axin2 and pcDNA-Flag-GSK3β plasmids have been described previously

[25]. The WT1 expression plasmid was generated by cloning the human WT1 coding sequence (NCBI Reference Sequence: NM_000378.4) into the pCDNA3.1 expression vector.

Cell culture and transient transfection

HEK293T and MCF-7 cells were cultured at 37°C with 5% CO2 in Dulbecco's modified Eagle's medium (Invitrogen, GIBCO, 11960) supplemented with 10% fetal calf serum, 1% penicillin/streptomycin and 2 mM glutamine (Invitrogen). For transient transfections, HEK293T cells were transfected with Fugene HD (Roche) and MCF-7 cells with PEI (polyethylenimine) or TransIT-TKO (Mirus, Madison, WI, USA) according to manufacturer's instructions.

Western Blotting and co-inmunoprecipitation

For analysis of protein expression, HEK293T cells were washed in ice-cold PBS and treated with RIPA lysis buffer containing a protease inhibitor cocktail (Roche) on ice for 1 h before harvesting, sonication and centrifugation at 12000 rpm for 20 min to remove cell debris. Cell lysates were boiled for 5 min in a 2X SDS standard sample buffer before being separated by electrophoresis on SDS-polyacrylamide gels. Proteins were then transferred to PVDF membrane (Bio-Rad). The membranes were blocked in PBS containing 5% non-fat dried milk for 3 h at room temperature (RT) before addition of the primary antibody and incubation, with agitation at 4°C overnight. After multiple washes with PBS, the membrane was incubated for 1 h in blocking buffer containing the appropriate HRP-conjugated secondary antibody (Promega).

Co-immunoprecipitation experiments were performed as described [8]. For WT1 co-immunoprecipitation Protein A/G Magnetic Beads (Pierce) were used.

Antibodies

The rabbit polyclonal antibody against WTX/AMER1 has been described previously [7].

Commercial antibodies used in this study were: chicken anti-GFP (Abcam, ab13970), rabbit anti-GFP (Abcam, ab290), mouse anti-GFP (Roche, mixture of clones 7.1 and 13.1), mouse anti-GAPDH (Santa Cruz, sc-32233), mouse anti-β-catenin (BD Transduction Laboratories, clone 14), rabbit anti-Axin1 (Cell Signalling, C76H11), rabbit anti-Axin2 (Cell Signalling, 76G6), rabbit anti-Gsk3β (Cell Signalling, 9315), rabbit anti-Flag (SIGMA F7425), mouse anti-Flag (SIGMA F3165), mouse anti-WT1 (Dako, M3561). Secondary antibodies were purchased from Jackson Immunoresearch.

Immunofluorescence

Axin1, Axin2 and Gsk3β were detected by immunofluorescence in transfected cells using anti-Flag or anti-Gsk3β antibodies as previously described [7]. GFP-WTX and GFP-WTX$^{flox\Delta}$ fusion proteins were detected by direct visualization of GFP fluorescence or by GFP immunofluorescence. Cells were fixed 48h after transfection for 10 min in 4% PFA and permeabilised with 0.1% Triton for 10 min at RT. After 1 hour blocking at RT in DMEM/10% FCS, the cells were incubated 1 hr with primary antibodies at RT, washed in PBS three times 5min at RT and then incubated with secondary antibodies for 1 h at RT in DMEM/10% FCS. Cells were washed in PBS, nuclei were stained with Hoechst (Invitrogen) and slides mounted with Mowiol. Photographs were taken as described in [7].

Skeletal staining and histology

For the alcian blue/alizarin red staining of whole newborn skeletons, mice were sacrificed, skinned, eviscerated, fixed in 95% ethanol and stained according to [26]. Photographs were taken on Zeiss Axio Zoom.V16 (Zeiss, Jena, Germany) with Zen software. Alcian blue/eosin staining on tissue sections was performed as described in [27].

X-ray and DEXA analysis and micro-CT

Adult mice were killed at 14 weeks of age by cervical dislocation, frozen, thawed, eviscerated skinned and fixed in 70% ethanol. Littermates for analysis (7 litters for *Wtx*$^{flox\Delta/+}$ males and 7 litters for *Wtx*$^{KO/+}$ females) were housed together and the following X-ray, DEXA and micro-CT analysis were performed in a blinded manner.

Mouse radiographs and DEXA scans were obtained with an UltraFocusDXA scanner (Faxitron Bioptics, Tucson, AZ USA) using standard protocols. Eviscerated carcasses were decapitated, with heads scanned using X-ray energy of 25 keV, 0.4 millamperes current for 10 seconds (9 micrometers pixel dimension) for measurements of skull dimensions. DEXA scans of the body (minus head) employed a pixel size of 16 micrometers with BMD parameters measured for the whole body and, using the ROI option, spine LV2 through LV5. Femurs and tibia were dissected from the carcasses and lengths measured with Vernier calipers. Spine lengths were measured radiographs. BMD parameters included Bone Area, BMD, BMD and vBMD (BMD divided by the square root of bone area), which adjusts BMD values for bone size [(28)]. Micro-CT analyses involved the use of a SKYSCAN 1272 scanner (Bruker, Coventry, UK). Bones were placed vertically and scanned with the settings: aluminum filter, 0.5 mm; resolution, 6 µm; energy, 70–90 kV; intensity, 100 µA; and integration time, 170 ms. Reconstruction of femurs and analysis of bone volume involved the use of CT analyser. The histomorphometric variables were expressed in compliance with the recommendation of the American Society for Bone and Mineral Research Histomorphometry Nomenclature Committee [(29)].

RNA assays

Total RNA from homogenized E11.5 embryos was isolated with the RNeasy Mini kit (Qiagen) following the manufacturer's instructions. cDNA was synthesized using a Superscript III first-strand cDNA synthesis kit (Invitrogen). *Wtx* relative expression levels were calculated as the ratio of the absolute quantifications, obtained by the standard curve method, between *Wtx* and the housekeeping gene *Hprt*. (Hprtp95_fw: tcctcctcagaccgctttt, Hprtp95_rs: ctggttcatcatcgctaatc; Wtxp84_fw: cagaggctccagctcaaatc, Wtxp84_rs: gcatcacagtggggtcct) using the LightCycler ® TaqMan ® Master system (Roche Applied Science).

Statistics

The number of embryos/adult animals for the different analysis are reported in the corresponding results section. Statistical analyses were performed using the GraphPad Prism v6 software. Statistical significance was assessed by the Mann-Whitney test or two-tailed Student's t-test

Results

Generation of two *Wtx* mutant alleles to study the *in vivo* role of WTX

To address the *in vivo* function of the C-terminal part of *WTX* and at the same time allow the generation of a loss-of-function allele, we inserted *loxP* sites upstream of exon 2 and at nucleotide position 1674 of the coding region (NCBI Reference Sequence: NP_780388.2) (Figure 1A**,** Suppl. Figure 1A, B**).** The presence of two stop codons within the *loxP* cassette is expected to lead to a truncated WTX$^{flox\Delta}$ protein that maintains the highly conserved N-terminal region, which is required for the interaction with APC and recruitment to the plasma membrane [7,8]. However, the truncated protein lacks the C-terminal domain that has been shown to interact with β-catenin via REA motifs [8] and WT1 [12] and appears to be necessary for nuclear localization. The second allele (*Wtx*^{KO}) was generated by Cre-mediated deletion of the *loxP* flanked sequences using a ubiquitously active Cre deleter (*Del-Cre* [21]) or an epiblast specific deleter strain (*Sox2-Cre* [22]). The Wtx^{KO} allele lacks the entire N-terminus of *Wtx* including splice acceptor regions and translation start site and thus should represent a null allele (Figure 1A, Suppl. Figure 1A). RT-PCR analysis on RNA isolated from E11.5 embryos showed normal splicing of the targeted allele in $\mathit{Wtx}^{flox\Delta}$, but failed to amplify a specific band in Wtx^{KO} mice, demonstrating that no *Wtx* transcript is produced from the KO allele (Suppl. Figure **1C**). Similarly, no amplification was observed by qRT-PCR with both a 5' intron spanning and 3' non-intron spanning primer sets on E13.5 embryos (Suppl. Figure **1D** and data not shown).

To evaluate the molecular properties of the truncated $\mathrm{WTX}^{\mathrm{flox}\Delta}$ protein we generated expression plasmids that mimic the *Wtx* wildtype and $\mathit{Wtx}^{flox\Delta}$ alleles, but carry a GFP-reporter fused to their N-terminal end. Western blotting with antibodies against GFP or WTX confirmed the presence of the predicted 217kDa and the 115kDa truncated protein in *GFP-Wtx* and *GFP-*$\mathit{Wtx}^{flox\Delta}$ transfected HEK293 cells, respectively (Suppl. Figure 1E). Analysis at the subcellular level revealed that GFP-WTX localized within the cytoplasm, at the plasma membrane and in 16% of cells in a speckled pattern within the nucleus, representing paraspeckles, as previously reported ([12] and data not shown). The truncated GFP-$\mathrm{WTX}^{\mathrm{flox}\Delta}$ protein maintained staining at the plasma membrane and to a lesser extent in the cytoplasm but showed much reduced nuclear localization (4%) (Figure 1B). These findings are consistent with the loss of the C-terminal nuclear translocation domain in the truncated GFP-$\mathrm{WTX}^{\mathrm{flox}\Delta}$ protein [12]. Pulldown experiments further demonstrated that the truncated protein was no longer able to interact with either of the two main alternatively spliced isoforms (+KTS and –KTS) of the Wilms' tumour suppressor WT1 (Figure 1C).

WTX can also directly interact with β-catenin and co-immunoprecipiation experiments in transfected HEK293 cells confirmed this interaction for the GFP-WTX protein (Figure 1D). By contrast, assays with the GFP-$\mathrm{WTX}^{\mathrm{flox}\Delta}$ plasmid showed that the truncated protein fails to precipitate co-transfected β-catenin, thus corroborating earlier findings that demonstrated a requirement of the C-terminal region of WTX for direct binding [8,9].

Taken together, these data indicate that *GFP-*$Wtx^{flox\Delta}$ results in a shorter protein that fails to enter the nucleus and cannot longer interact with WT1 or β-catenin.

Calvarial and midline developmental defects in *Wtx* mutant alleles

We next addressed the *in vivo* function of the newly generated alleles (Suppl. Figure 2A-C). Both Wtx^{KO} and $Wtx^{flox\Delta}$ animals were born at the expected Mendelian rates (Suppl. Figure 2D, E). As reported previously [19], Wtx^{KO} males (XY Wtx^{KO}) died soon after birth and displayed somatic overgrowth and increased body mass compared to controls (Figure 2A, B, Suppl. Figure 2F). By contrast, $Wtx^{flox\Delta}$ males were viable, fertile and produced offspring (Figure 2B, Suppl. Figure 2G), demonstrating that deletion of the C-terminal half of *Wtx* ($Wtx^{flox\Delta}$ allele) was compatible with postnatal life.

During development, *Wtx* is expressed in the metanephric mesenchyme surrounding the branching epithelium [6,30], and thus would be active in the progenitor cell population that is supposed to give rise to Wilms' tumour. We did not observe the development of kidney tumours in $Wtx^{flox\Delta}$ or $Wtx^{KO/+}$ adult mice, but inspection of the urogenital region between E13.5 and birth revealed unilateral or bilateral renal agenesis in up to 62% of Wtx^{KO} mice analysed (Suppl. Figure 2I). As reported previously [19], this phenotype appeared to be genetic background dependent. Kidney development in $Wtx^{flox\Delta}$ mutants was indistinguishable from wildtype littermates (data not shown).

To further assess the importance of the C-terminal domain of WTX during skeletal development, we decided to perform a detailed comparison between our male Wtx^{KO} and $Wtx^{flox\Delta}$ alleles. As WTX is an X-linked gene for which males are constitutively hemizygous, we focused our developmental analysis on male mice, thus limiting the inherent variability observed in heterozygote females due to different in X-inactivation ratios. Close examination of Wtx^{KO} skulls at birth revealed a number of skeletal developmental defects including the presence of a complete cleft palate in 43% of the mutants (Figure 2C, and Suppl. Figure 2J) and milder fusion defects of the palatal shelves in the remaining mutants (see below). Since cleft palate is incompatible with the survival of newborn mice, this could explain in part the cyanosis, lack of milk in the stomach and perinatal lethality in 100% of Wtx^{KO} mice (n=58, Figure 2B). In addition, Wtx^{KO} mice showed an overall shortening of the skull and an increase in the width to length skull ratio (Figure 2D, E). To evaluate whether the altered skull proportions maybe due to premature ossification of skull bones, we isolated calvarial osteoblasts from P0 pups and analysed their differentiation potential *in vitro*. Surprisingly, *Wtx* knockout osteoblasts showed a significant decrease rather than an increase in the formation of alizarin red stained bone nodules, thus excluding premature ossification as an explanation for the observed phenotype (Suppl. Figure 2K). However, further inspection of the base of the skulls revealed a bony bridge connecting the basioccipitale with the basisphenoid bone, which could explain the altered skull proportions observed in Wtx^{KO} mice (Figure 2F). This phenotype was accompanied by the presence of a hole or cleft in the posterior region of the basisphenoid bone in more than 90% of the mutants analysed (n=13) (Figure 2F). Finally, examination of the base of the skull also helped distinguish palatal clefts of different severity not detected by visual inspection of the oral cavity at birth. In the less severe cases, the palatal processes of the incisive and maxillary bones failed to extend and juxtapose at the midline (Figure 2F'). In cases of a full cleft, the palatal processes of the maxillary and palatine bones were severely hypoplastic and allowed visualization of the presphenoid and vomer bones (Figure 2F'', 2G). In contrast, $Wtx^{flox\Delta}$ mice displayed normal palate development and a very mild skull phenotype. Only 30% of $Wtx^{flox\Delta}$ mice (n=10) presented a thin bony bridge connecting the basioccipitale with the basisphenoid bones (Figure 2F), probably explaining the less severe increase in the skull proportions (3%), when compared to the increase of *Wtx*^{KO} animals (8%) versus wildtype controls (Figure 2D, E).

Examination of the remaining skeleton confirmed previous observations and revealed a number of additional skeletal defects (Suppl. Table 1). *Wtx*^{KO} pups presented a reduced or absent deltoid tuberosity (100%; Figure 3A), split lumbar vertebral bodies (61%, Figure 3B), and a pronounced alteration in spine curvature at the cervical level (100%, Suppl. Figure 2L). All *Wtx*^{KO} pups analysed (n=13) displayed a split sternum, where the sternal bars where not fused at the midline (100%, Figure 3C). The xiphoid process of the developing sternum was also abnormally bifurcated with two separate ossification centres remaining in some *Wtx*^{KO} pups. *Wtx*$^{flox\Delta}$ mice did not present these abnormalities, but displayed more subtle patterning defects (n=10). The deltoid tuberosity was present, but appeared misshapen in *Wtx*$^{flox\Delta}$ mice (Figure 3A). At the level of the developing sternum, fusion of the lower part of the sternal bars seemed to be delayed and fusion of the xiphoid process was incomplete in 30% of the *Wtx*$^{flox\Delta}$ mice analysed (Figure 3C). Finally, measurements along the anterior-posterior axis revealed that *Wtx*^{KO} mutant sterni were shortened, with the length of the ossified part of the manubrium being most severely affected (Figure 3D). However, no significant change was found in *Wtx*$^{flox\Delta}$ mice. Overall, our phenotypic comparison during development at all anatomical locations between our two WTX alleles, reveal a milder phenotype when the truncated WTX$^{flox\Delta}$ protein is present.

The WTX$^{flox\Delta}$ protein is able to interact indirectly with β-catenin via Axin

In order to address whether the skeletal defects described above were due to dysregulated β-catenin levels, we attempted to complement our complete *Wtx* mutants with a *β-catenin* loss of function allele [(23)]. Reduction in β-catenin gene dosage, partially rescued survival at P0 (Suppl. Figure 3A, 58% survival, n=12), and improved the calvarial proportions and sternal fusion defects due to *Wtx* deficiency (Suppl. Figure 3B**, C).** Therefore, this result confirmed the previous observations [19] indicating that the relative abundance of these two proteins has to be tightly balanced during skeletal development. On this basis, the less severe phenotype in XY *Wtx^floxΔ^* animals, when compared to a complete knockout (XY *Wtx^KO^)*, was surprising given the proposed function of WTX as a negative regulator of β-catenin and the fact that the truncated WTX protein is unable to directly bind β-catenin (Figure 1D). Therefore, we decided to perform additional molecular analyses of the $WTX^{flox\Delta}$ protein. Previous *in vitro* studies suggested that WTX may exert its function by interacting with β-catenin and GSK3β indirectly through its association with the scaffolding proteins of the β-catenin degradation complex AXIN1/AXIN2 [10]. To test whether the $WTX^{flox\Delta}$ protein was still able to bind to these proteins, we performed co-transfection assays in HEK293 cells. In this setting, both WTX and $WTX^{flox\Delta}$ were able to interact with overexpressed AXIN2 as demonstrated by co-inmunoprecipitation experiments. In addition, both proteins were able to pull-down endogenous GSK3β and β-catenin in the presence of overexpressed AXIN1 or AXIN2 (Figure 4A, Suppl. Figure 4A and data not shown). We could confirm these results by immuno-fluorescent microscopy on transfected MCF7 cells. $WTX^{flox\Delta}$ protein was still able to recruit both AXIN1 and AXIN2 to the cell membrane (Figure 4B, Suppl. Figure 4B). Similarly, the $WTX^{flox\Delta}$ protein was able to relocate GSK3β from its diffuse cytoplasmic localization to the membrane in the presence, but not in the absence of overexpressed AXIN2 (Figure 4C, D). However, close inspection suggested that the recruitment of AXIN1 from its characteristic cytoplasmic puncta [31] by $WTX^{flox\Delta}$ protein was slightly less efficient when compared to wildtype WTX (Figure 4D, Suppl Figure 4B). We conclude that the C-terminal domain of WTX is dispensable for survival and that – at least *in vitro* - the truncated $WTX^{flox\Delta}$ protein is still able to indirectly interact with β-catenin and recruit GSK3β to the membrane via its interaction with AXIN1/2, albeit in a slightly less efficient manner.

Truncation mutations cause increased bone mass density as observed in human patients

Survival of XY *Wtx*$^{flox\Delta}$ mice beyond birth (Suppl. Figure 2G) permitted us to examine the effect of C-terminal truncations on bone development in adults (14 weeks). For comparison, we also analysed XX *Wtx*$^{KO/+}$mice, which generally showed a more variable phenotype with a proportion of mice dying at birth (21.6%, n=37, Figure 2B). This variability is probably due to the stochastic nature of X-inactivation, which in certain *Wtx*$^{KO/+}$ embryos may result in the predominant inactivation of the wildtype *Wtx* allele, thus leading to an effective null phenotype and perinatal death. However, most heterozygote *Wtx*$^{KO/+}$ females were viable, fertile (Suppl. Figure 2H) and could be used in the analysis. No significant differences in body weight were observed between either XY *Wtx*$^{flox\Delta}$ or XX *Wtx*$^{KO/+}$mice and their respective littermate controls (Suppl. Figure 5A).

Surviving *Wtx*$^{KO/+}$ females and some *Wtx*$^{flox\Delta}$ males displayed a noticeable shortening and dome-shaped appearance of the head that was more severe in the case of mutant females (Figure 5A, B, and data not shown). This morphological feature permitted an easy identification of the *Wtx* heterozygous females among their wildtype littermates within the first 3 weeks after birth. Measurements of skulls after X-ray analysis revealed a significant increase in the width/length ratio in both XY *Wtx*$^{flox\Delta}$ (11%; n=11) and XX *Wtx*$^{KO/+}$ (18%; n=12) over control animals (Figure 5C, Suppl. Figure 5B, C). The altered skull architecture in mutant mice appeared to affect all bones proportionally, as no incisor malocclusions were observed.

No bone striations similar to those observed in OSCS patients were observed in radiographs of spine, femur or tibia of *Wtx*$^{KO/+}$ females (Suppl. Figure 5D and data not shown). In addition, analysis of femur, tibia and spinal column showed no significant length changes in XY *Wtx*$^{flox\Delta}$ and XX *Wtx*$^{KO/+}$ animals when compared to controls (Suppl. Figure 5E). However, dual energy X-ray absorptiometry (DEXA) scans revealed similar elevations of volumetric bone mass density (vBMD) in the whole body of *Wtx*$^{flox\Delta}$ male (+8%) and *Wtx*$^{KO/+}$ female mice (+7%) (Figure 5D).

To analyze the bone phenotype further, we carried out microcomputed tomography (micro-CT) at the level of the distal femoral metaphysis. A small, but significant increase in trabecular bone volume to total bone volume ratio (BV/TV) was observed at the femur of *Wtx*$^{flox\Delta}$ male mice (+4.5%) (Figure 5E). The BV/TV of *Wtx*$^{KO/+}$ female mice at the femur levels was not significantly different from WT values, probably due to the higher phenotypic variability due to X-inactivation in females. The cortical and trabecular thickness did not exhibit statistically significant alterations in neither *Wtx*$^{flox\Delta}$ male or *Wtx*$^{KO/+}$ female mice compared to controls. However, truncation or heterozygote mutations in *Wtx* seemed to affect the trabecular bone architecture. *Wtx*$^{flox\Delta}$ male mice showed reduced trabecular separation and increased trabecular number compared to controls. In addition, bone trabeculae in *Wtx*$^{flox\Delta}$ mice were more “plate-like”, as revealed by the reduced structure model index, thus suggesting changes in trabecular orientation. Similar though less marked trends were observed for these parameters in *Wtx*$^{KO/+}$ female mice. Taken together, these analyses suggest that genetic inactivation of *Wtx* resulted in an increase in bone mass, which was more evident in males.

Discussion

OSCS is an X-linked disease characterized by a wide variety of skeletal defects due to germline mutations in *WTX*. The clinical symptoms vary greatly among female patients most likely due to variability in the ratio of random X-inactivation of the remaining wildtype *WTX* allele. In addition to this epigenetic variability, the phenotype appears to be also influenced by the type of mutation within *WTX*. Whereas gene deletions or nonsense mutations at the 5 ' end of the gene are almost always lethal in male patients, truncations that affect the 3' end generally have a less severe phenotype permitting survival till adulthood [14,17], although it should be noted that this genotype-phenotype relationship is not absolute [15,32]. The mutant alleles generated in the present study provide us with important additional functional information, both on the developmental and molecular level.

A defining feature of the mutant phenotype in Wtx^{KO} mice appears to be the midline defects including severe abnormalities in the sternum, vertebrae and the palate. While several of these phenotypes have been reported in a previous study [19], our analysis revealed additional defects in skull bone architecture including cleft palate and abnormal development of the base of the skull. Palatogenesis, the developmental process that forms the intact roof of the oral cavity, is often disrupted by genetic and environmental perturbations, as reflected in the high frequency of cleft palate in humans [33]. Since cleft palates are incompatible with the postnatal survival of mice, this phenotype is a likely cause of the observed perinatal lethality in male *Wtx* knockout animals. Of note, complete cleft palate was observed in only 43% of the male Wtx^{KO} analysed, and the severity of clefting seemed to be influenced by the genetic background of the mice (increased penetrance of the full cleft when the line was in a C57BL/6 background compared to a 129SV background), an observation previously documented for other mutations [34].

Previous studies have already demonstrated that β-catenin must be tightly regulated to permit normal palate development and both loss- and gain-of-function experiments in the palatal epithelia results in failure of palatal shelf fusion [35,36]. WTX exerts its negative regulatory role in WNT signalling by interacting with key components of the β-catenin destruction complex, including APC, AXIN proteins, β-catenin and GSK3β [8,9]. Interestingly, targeted disruption of *Gsk3β*, an important kinase targeting β-catenin for destruction, also causes cleft palate and sternal fusion defects [37,38]. Although GSK3β is considered a promiscuous kinase that can affect a wide variety of other pathways [39], the similar phenotype with *Wtx* mutants and the fact that WTX is required for the recruitment of GSK3β to the membrane via the interaction with AXIN1 or AXIN2 ([10] and this study) would argue that WTX is essential for GSK3β to exert its function *in vivo* in a β-catenin dependent context. It raises also the interesting possibility that GSK3β would require membrane localization for its function during skeletal development. Interestingly, at least at the palatal level, inactivation of *Gsk3β* does not seem to affect WNT/β-catenin reporter activity despite being expressed primarily in epithelial layers overlapping with β-catenin [38]. Therefore, the mechanistic role of GSK3β in this context remains unclear. Similarly, given that WTX can function in either the canonical WNT signalling pathway [9] or as a component of adherens junctions together with β-catenin [7], further studies will be required to understand the precise cellular role of these proteins in palatal development.

Apart from the palatal abnormalities, we also noticed a hole in the middle or posterior region of the basisphenoid bone. A similar phenotype in the basisphenoid bone has been reported in a number of mutant mice [40-43] including components of the WNT signalling pathway [27,44]. In addition, we also observed an ectopic ossified bridge connecting the basioccipitale with the basisphenoid bone at the base of the skull at the level of the spheno-occipital synchondrosis. In the cranial base synchondroses, i.e the sutures between the bones of the skull base that serve as endochondral growth sites, a fine balance between proliferation and differentiation of chondrocytes takes place that allows embryonic and postnatal growth of the skull [45,46]. A phenotype characterized by shortened, dome-shaped skulls has been described previously for other mutants [27,45,47-49] and related to the presence of a bony bridge at this level. Since experimentally induced fusion of the base of the skull causes craniofacial shortening [50], it is likely that ectopic synostosis is also responsible for the skull dysmorphisms observed in Wtx^{KO} mice. Importantly, the craniofacial phenotype in Wtx^{KO} and $Wtx^{flox\Delta}$ mice strongly correlates with the dysmorphism seen in OSCS patients that often display cleft palate, macrocephaly and frontal or occipital bossing of the skull [14,15,17]. To our knowledge, the presence of bony bridges at the base of the skull has not been reported in OSCS patients, but in the light of our results it may be worth to revisit this possibility.

In addition to our Wtx^{KO} loss-of-function model that results in perinatal lethality, we also described here a less severely affected $Wtx^{flox\Delta}$ allele that produces a truncated version of the WTX protein. Human patients with truncation mutations at a comparable position also survive and show a range of skeletal anomalies that are highly similar to those found in our mouse model including macrocephaly, frontal bossing, high arched and cleft palate and severe bone sclerosis [14,15,17]. The overlapping, but less severe phenotype of $Wtx^{flox\Delta}$ mice, when compared to the loss-of-function allele (XY Wtx^{KO}) during development, is in agreement with the truncated protein acting as a hypomorph, a hypothesis that has already been put forward for human truncation mutations [14] and is further supported by our *in vitro* studies.

When compared to the Wtx^{KO} allele, the developmental defects in $Wtx^{flox\Delta}$ mutants are relatively mild despite the fact that the truncated protein no longer co-immunoprecipitates with β-catenin. The C-terminal domain of WTX contains so-called REA repeats that are important for direct interaction with β-catenin [10]. This motif lies outside the conserved blocks of sequences identified in all WTX orthologues [24] and does not appear to be highly conserved throughout evolution. It is, therefore, likely that mammals have adopted the REA motif to increase the affinity of WTX to β-catenin [10]. The less severe phenotype of the $Wtx^{flox\Delta}$ mutant mice during development could be explained by an indirect interaction of the truncated protein with β-catenin via AXIN1 and AXIN2 thus retaining a certain degree of WTX function. However, the increased BMD phenotype observed in $Wtx^{flox\Delta}$ adult mice suggests that this association is inefficient and that the C-terminal domain of WTX is required to fine-tune WNT signalling. Confirming this model *in vivo* is however difficult, as the low amounts of protein do not allow efficient co-precipitation.

The fact that reducing β-catenin levels rescues to a certain extent the *Wtx* full knockout phenotype in mice ([19], our data) strongly argues that also *in vivo* one of the primary functions of WTX is to diminish the protein levels of this gene. However, as mentioned before, WTX has been shown to also stabilize adherens junctions in epithelial cell lines *in vitro*, probably by recruiting APC to the membrane [7]. Thus, it is currently unclear whether the rescue is strictly due to the re-establishment of appropriate levels of WNT/β-catenin signalling or caused by other coincident effects exerted by WTX and β-catenin at the plasma membrane. In addition, given that those *WTX* truncation mutations that retain at least one APC binding domain and membrane binding capability result in a milder phenotype (as in our $Wtx^{flox\Delta}$ allele), the membrane localization of WTX was suggested to be protective against the disease [14]. Therefore, analysis of changes in the stability of cell adhesions and levels of transcriptionally active β-catenin might help understanding the relevance of these different functions of WTX in different cellular contexts.

Bone mass is regulated by a tight balance between the activities of bone-forming osteoblasts and bone-resorbing osteoclasts. Osteocytes, i.e. terminally differentiated osteoblasts embedded in the mineralized bone matrix, maintain bones and coordinate the action of osteoblasts and osteoclasts during bone modelling and remodelling [51]. The sclerosing aspect of several bones is the most prominent feature of OSCS**.** Therefore, we performed DEXA and micro-CT analysis in adult Wtx^{flox} males and $Wtx^{KO/+}$ heterozygous females, as they survived beyond birth. Similarly to the human condition, we observed a significant**,** although milder increase in vBMD in adult $Wtx^{flox\Delta}$ male and $Wtx^{KO/+}$ female mice. A key feature for OSCS is that sclerosis is accompanied by linear striations in the metaphyseal region of the long bones of female patients [14,16]. Male patients generally do not show metaphyseal striations, with the exceptions of those carrying a mosaic mutation [17]. While at present there is no proven explanation for the origin of the striations, variation in bone formation rate due to non-random X inactivation was proposed as a potential mechanism for the phenotype [52,53]. Interestingly, *Osteopathia striata* also occurs in patients with focal dermal hypoplasia resulting from mutations in the X-linked gene *PORCN*, an enzyme required for WNT protein modification and secretion [54]. However, in contrast to the human condition, *Wtx* mouse mutants do not show striations of the long bones in adulthood up to 4 months of age ([19] and this study). This may suggest that changes in bone density caused by *Wtx* or *Porcn* mutations are less severe in mice than in men and thus not detectable by X-ray analysis. Alternatively, the spatial pattern of X-inactivation in bone progenitors during development might differ between human and mice.

A large number of studies have demonstrated that sustained WNT signalling, in particular the canonical WNT pathway, induces an overall increase in bone mass. The hyperostotic phenotypes caused by sustained β-catenin activity have been variably attributed to different cellular mechanisms: enhanced commitment towards the osteoblastic lineage, increased osteoblast activity and inhibition of osteoclast differentiation (reviewed by [51,55]). However, the relative impact on bone formation and resorption seems to depend on the developmental context and timing of activation of canonical WNT signalling in the different models. A previous report has provided compelling evidence that the bone overgrowth phenotype in *Wtx* mutants is at least partly due to an increased commitment of mesenchymal progenitors to the osteoblast lineage followed by a subsequent delay in the terminal differentiation of committed osteoblasts [19]. While we have not analysed the dynamics of bone mesenchymal progenitors during development in our mutant mice, our micro-CT analysis has also revealed a moderate increase in the bone volume fraction in the femur of adult $Wtx^{flox\Delta}$ male mice. Interestingly, our analysis revealed no change of cortical or trabecular thickness, which would suggest normal bone formation in our mutant animals. By contrast, we observed a significant reduction of trabecular spacing in our micro-CT analysis of $Wtx^{flox\Delta}$ male mice. An increase in the trabecular number in combination with reduced trabecular spacing is indicative for a decreased osteoclast activity. This may suggest that the increased bone mass in our mutants is due to decreased bone resorption rather than increased bone formation. While the reasons for the discrepancies with the previous report [19] are unclear, it is worth mentioning the inherent differences of both analyses. Moisan et al. analysed 6 week-old male mice in which *Wtx* had been inactivated in skeletal mesenchymal cells (using the *Prx1-Cre* line) or in osteoblast precursors (*Osterix-Cre* line) [19]. β-catenin signalling is known to regulate the coupling of osteoblasts with osteoclast precursors, by controlling expression of osteoprotegerin (Opg), a competitive inhibitor of Rankl and Rank interaction [55]. While the inactivation of *Wtx* in osteoblasts did not seem to affect osteoclast activity or numbers, the cell autonomous role of *Wtx* in osteoclasts, which derive from the hematopoietic lineage [56], has not been addressed. Conversely, in our study, we analysed germline *Wtx* mutations in 14 week-old mice (*Wtx* truncation mutation in male or heterozygote mutation in female mice), which may impact simultaneously on both osteoblast and osteoclast biology. It will therefore be interesting to perform osteoclast specific deletion of *Wtx* to address a potential direct role of *Wtx* in regulating the differentiation and function of this cell type. Finally, sex and age-dependent changes in bone microarchitecture [57], as well as differences in the genetic background [58] could contribute to differences in the two models. Importantly, neither of the available *Wtx* mutant mouse models ([19], this study) fully phenocopied a β-catenin gain-of-function mutation or mutations on other negative regulators of the WNT/ β-catenin pathway [51,55]. This probably reflects the complex fine tuning of the WNT regulatory network and highlights potential β-catenin independent and stage-specific functions of WTX as suggested previously [19].

In summary, we described here two novel WTX alleles that vary in severity, ranging from a milder survivable form ($Wtx^{flox\Delta}$) in males to a severe and perinatal lethal one (Wtx^{KO}). Our novel $Wtx^{flox\Delta}$ allele constitutes a mouse model for OSCS that largely recapitulates the phenotype found in patients carrying truncation mutations. Thus, this strain will be a useful model to further study the molecular and cellular mechanisms leading to the phenotype and to test whether osteosclerosis can be ameliorated through therapeutic approaches.

Acknowledgements

The authors thank Sebastien Schaub for assistance in confocal microscopy and Morgane Bourmaud for micro-CT scans. We are grateful to Marie-Christine Chaboissier and Anne-Amandine Chassot for providing mice and helpful discussions. We would like to thank A. Kikuchi for the pcDNA-Flag-Axin1 construct and Dr Holger Scholz (Charité-Universitätsmedizin, Berlin) for the plasmid containing human WT1 cDNA. A.B. and G.C. were supported by ARC (French agency for cancer research) and a Marie-Curie fellowship. This work was supported by grants from ARC (grant 1130) and the Association for International Cancer Research (AICR grant 09-0752) to A.S and by the German Federal Ministry of Education and Research (Infrafrontier grant 01KX1012) to MHdA. J.B. and K.T. were supported by a grant from the Deutsche Forschungsgemeinschaft BE1550/6-1 to JB.

Authors' roles: Study design: GC and AS. Data collection and analysis: GC, AB, KT, ASR, FM, AC, CP, FJM. RB and WH performed X-ray/DEXA analysis. MCS and TFB performed CT-scans. Data interpretation: GC, CH, JB, MCS and AS. Drafting manuscript: AS and GC. Approving final version of manuscript: all authors. AS takes responsibility for the integrity of the data analysis.

References

1. MacDonald BT, Tamai K, He X. Wnt/beta-catenin signaling: components, mechanisms, and diseases. Dev Cell. Jul 2009;17(1):9-26. Epub 2009/07/22.
2. Clevers H. Wnt/beta-catenin signaling in development and disease. Cell. Nov 3 2006;127(3):469-80.
3. Angers S, Moon RT. Proximal events in Wnt signal transduction. Nat Rev Mol Cell Biol. Jul 2009;10(7):468-77. Epub 2009/06/19.
4. Reya T, Clevers H. Wnt signalling in stem cells and cancer. Nature. Apr 14 2005;434(7035):843-50. Epub 2005/04/15.
5. Huff V. Wilms' tumours: about tumour suppressor genes, an oncogene and a chameleon gene. Nat Rev Cancer. Feb 2011;11(2):111-21. Epub 2011/01/21.
6. Rivera MN, Kim WJ, Wells J, Driscoll DR, Brannigan BW, Han M, et al. An X chromosome gene, WTX, is commonly inactivated in Wilms tumor. Science. Feb 2 2007;315(5812):642-5.
7. Grohmann A, Tanneberger K, Alzner A, Schneikert J, Behrens J. AMER1 regulates the distribution of the tumor suppressor APC between microtubules and the plasma membrane. J Cell Sci. Nov 1 2007;120(Pt 21):3738-47. Epub 2007/10/11.
8. Tanneberger K, Pfister AS, Kriz V, Bryja V, Schambony A, Behrens J. Structural and functional characterization of the Wnt inhibitor APC membrane recruitment 1 (Amer1). J Biol Chem. Jun 03 2011;286(22):19204-14.
9. Major MB, Camp ND, Berndt JD, Yi X, Goldenberg SJ, Hubbert C, et al. Wilms tumor suppressor WTX negatively regulates WNT/beta-catenin signaling. Science. May 18 2007;316(5827):1043-6.
10. Tanneberger K, Pfister AS, Brauburger K, Schneikert J, Hadjihannas MV, Kriz V, et al. Amer1/WTX couples Wnt-induced formation of PtdIns(4,5)P2 to LRP6 phosphorylation. EMBO J. Apr 20 2011;30(8):1433-43.
11. Zhang Z, Akyildiz S, Xiao Y, Gai Z, An Y, Behrens J, et al. Structures of the APC-ARM domain in complexes with discrete Amer1/WTX fragments reveal that it uses a consensus mode to recognize its binding partners. Cell Discov. 2015;1:15016.
12. Rivera MN, Kim WJ, Wells J, Stone A, Burger A, Coffman EJ, et al. The tumor suppressor WTX shuttles to the nucleus and modulates WT1 activity. Proc Natl Acad Sci U S A. May 19 2009;106(20):8338-43. Epub 2009/05/07.
13. Kim WJ, Rivera MN, Coffman EJ, Haber DA. The WTX tumor suppressor enhances p53 acetylation by CBP/p300. Molecular cell. Mar 9 2012;45(5):587-97.
14. Jenkins ZA, van Kogelenberg M, Morgan T, Jeffs A, Fukuzawa R, Pearl E, et al. Germline mutations in WTX cause a sclerosing skeletal dysplasia but do not predispose to tumorigenesis. Nat Genet. Jan 2009;41(1):95-100. Epub 2008/12/17.
15. Perdu B, de Freitas F, Frints SG, Schouten M, Schrander-Stumpel C, Barbosa M, et al. Osteopathia striata with cranial sclerosis owing to WTX gene defect. J Bone Miner Res. Jan 2010;25(1):82-90.
16. Pellegrino JE, McDonald-McGinn DM, Schneider A, Markowitz RI, Zackai EH. Further clinical delineation and increased morbidity in males with osteopathia striata with cranial sclerosis: an X-linked disorder? Am J Med Genet. May 16 1997;70(2):159-65.
17. Holman SK, Daniel P, Jenkins ZA, Herron RL, Morgan T, Savarirayan R, et al. The male phenotype in osteopathia striata congenita with cranial sclerosis. Am J Med Genet A. Oct 2011;155A(10):2397-408.
18. Hartmann C. A Wnt canon orchestrating osteoblastogenesis. Trends Cell Biol. Mar 2006;16(3):151-8. Epub 2006/02/10.

19. Moisan A, Rivera MN, Lotinun S, Akhavanfard S, Coffman EJ, Cook EB, et al. The WTX tumor suppressor regulates mesenchymal progenitor cell fate specification. Dev Cell. May 17 2011;20(5):583-96.
20. Nagy A, Rossant J, Nagy R, Abramow-Newerly W, Roder JC. Derivation of completely cell culture-derived mice from early-passage embryonic stem cells. Proc Natl Acad Sci U S A. Sep 15 1993;90(18):8424-8. Epub 1993/09/15.
21. Schwenk F, Baron U, Rajewsky K. A cre-transgenic mouse strain for the ubiquitous deletion of loxP-flanked gene segments including deletion in germ cells. NucleicAcidsRes. // 1995;23(24):5080-1.
22. Hayashi S, Lewis P, Pevny L, McMahon AP. Efficient gene modulation in mouse epiblast using a Sox2Cre transgenic mouse strain. Gene Expr Patterns. Nov 2002;2(1-2):93-7.
23. Brault V, Moore R, Kutsch S, Ishibashi M, Rowitch DH, McMahon AP, et al. Inactivation of the beta-catenin gene by Wnt1-Cre-mediated deletion results in dramatic brain malformation and failure of craniofacial development. Development. Apr 2001;128(8):1253-64.
24. Boutet A, Comai G, Schedl A. The WTX/AMER1 gene family: evolution, signature and function. BMC Evol Biol. 2010;10:280. Epub 2010/09/17.
25. Behrens J, Jerchow BA, Wurtele M, Grimm J, Asbrand C, Wirtz R, et al. Functional interaction of an axin homolog, conductin, with beta-catenin, APC, and GSK3beta. Science. Apr 24 1998;280(5363):596-9. Epub 1998/05/09.
26. McLeod MJ. Differential staining of cartilage and bone in whole mouse fetuses by alcian blue and alizarin red S. Teratology. Dec 1980;22(3):299-301.
27. Lyashenko N, Weissenbock M, Sharir A, Erben RG, Minami Y, Hartmann C. Mice lacking the orphan receptor ror1 have distinct skeletal abnormalities and are growth retarded. Dev Dyn. Aug 2010;239(8):2266-77.
28. Carter DR, Bouxsein ML, Marcus R. New approaches for interpreting projected bone densitometry data. J Bone Miner Res. Feb 1992;7(2):137-45.
29. Bouxsein ML, Boyd SK, Christiansen BA, Guldberg RE, Jepsen KJ, Muller R. Guidelines for assessment of bone microstructure in rodents using micro-computed tomography. J Bone Miner Res. Jul 2010;25(7):1468-86.
30. Comai G, Boutet A, Neirijnck Y, Schedl A. Expression patterns of the Wtx/Amer gene family during mouse embryonic development. Dev Dyn. Jun 2010;239(6):1867-78. Epub 2010/05/27.
31. Fagotto F, Jho E, Zeng L, Kurth T, Joos T, Kaufmann C, et al. Domains of axin involved in protein-protein interactions, Wnt pathway inhibition, and intracellular localization. J Cell Biol. May 17 1999;145(4):741-56.
32. Perdu B, Lakeman P, Mortier G, Koenig R, Lachmeijer AM, Van Hul W. Two novel WTX mutations underscore the unpredictability of male survival in osteopathia striata with cranial sclerosis. Clin Genet. Oct 2011;80(4):383-8.
33. Bush JO, Jiang R. Palatogenesis: morphogenetic and molecular mechanisms of secondary palate development. Development. Jan 2012;139(2):231-43.
34. Proetzel G, Pawlowski SA, Wiles MV, Yin M, Boivin GP, Howles PN, et al. Transforming growth factor-beta 3 is required for secondary palate fusion. Nat Genet. Dec 1995;11(4):409-14.
35. Funato N, Nakamura M, Yanagisawa H. Molecular basis of cleft palates in mice. World J Biol Chem. Aug 26 2015;6(3):121-38.
36. He F, Xiong W, Wang Y, Li L, Liu C, Yamagami T, et al. Epithelial Wnt/beta-catenin signaling regulates palatal shelf fusion through regulation of Tgfbeta3 expression. Dev Biol. Feb 15 2011;350(2):511-9.

37. Liu KJ, Arron JR, Stankunas K, Crabtree GR, Longaker MT. Chemical rescue of cleft palate and midline defects in conditional GSK-3beta mice. Nature. Mar 1 2007;446(7131):79-82. Epub 2007/02/13.
38. He F, Popkie AP, Xiong W, Li L, Wang Y, Phiel CJ, et al. Gsk3beta is required in the epithelium for palatal elevation in mice. Dev Dyn. Dec 2010;239(12):3235-46.
39. Frame S, Cohen P. GSK3 takes centre stage more than 20 years after its discovery. Biochem J. Oct 1 2001;359(Pt 1):1-16. Epub 2001/09/21.
40. Baffi MO, Slattery E, Sohn P, Moses HL, Chytil A, Serra R. Conditional deletion of the TGF-beta type II receptor in Col2a expressing cells results in defects in the axial skeleton without alterations in chondrocyte differentiation or embryonic development of long bones. Dev Biol. Dec 01 2004;276(1):124-42.
41. Jena N, Martin-Seisdedos C, McCue P, Croce CM. BMP7 null mutation in mice: developmental defects in skeleton, kidney, and eye. Exp Cell Res. Jan 10 1997;230(1):28-37.
42. Holst CR, Bou-Reslan H, Gore BB, Wong K, Grant D, Chalasani S, et al. Secreted sulfatases Sulf1 and Sulf2 have overlapping yet essential roles in mouse neonatal survival. PLoS One. Jun 27 2007;2(6):e575.
43. Bose J, Grotewold L, Ruther U. Pallister-Hall syndrome phenotype in mice mutant for Gli3. Hum Mol Genet. May 01 2002;11(9):1129-35.
44. Brugmann SA, Goodnough LH, Gregorieff A, Leucht P, ten Berge D, Fuerer C, et al. Wnt signaling mediates regional specification in the vertebrate face. Development. Sep 2007;134(18):3283-95.
45. Kolpakova-Hart E, McBratney-Owen B, Hou B, Fukai N, Nicolae C, Zhou J, et al. Growth of cranial synchondroses and sutures requires polycystin-1. Dev Biol. Sep 15 2008;321(2):407-19.
46. McBratney-Owen B, Iseki S, Bamforth SD, Olsen BR, Morriss-Kay GM. Development and tissue origins of the mammalian cranial base. Dev Biol. Oct 01 2008;322(1):121-32.
47. Eswarakumar VP, Monsonego-Ornan E, Pines M, Antonopoulou I, Morriss-Kay GM, Lonai P. The IIIc alternative of Fgfr2 is a positive regulator of bone formation. Development. Aug 2002;129(16):3783-93.
48. Dabovic B, Chen Y, Colarossi C, Obata H, Zambuto L, Perle MA, et al. Bone abnormalities in latent TGF-[beta] binding protein (Ltbp)-3-null mice indicate a role for Ltbp-3 in modulating TGF-[beta] bioavailability. J Cell Biol. Jan 21 2002;156(2):227-32.
49. Dabovic B, Chen Y, Colarossi C, Zambuto L, Obata H, Rifkin DB. Bone defects in latent TGF-beta binding protein (Ltbp)-3 null mice; a role for Ltbp in TGF-beta presentation. J Endocrinol. Oct 2002;175(1):129-41.
50. Rosenberg P, Arlis HR, Haworth RD, Heier L, Hoffman L, LaTrenta G. The role of the cranial base in facial growth: experimental craniofacial synostosis in the rabbit. Plast Reconstr Surg. Apr 1997;99(5):1396-407.
51. Baron R, Kneissel M. WNT signaling in bone homeostasis and disease: from human mutations to treatments. Nat Med. Feb 2013;19(2):179-92.
52. Viot G, Lacombe D, David A, Mathieu M, de Broca A, Faivre L, et al. Osteopathia striata cranial sclerosis: non-random X-inactivation suggestive of X-linked dominant inheritance. Am J Med Genet. Jan 01 2002;107(1):1-4.
53. Kraus C, Konig R, Rott HD. Comments on "osteopathia striata cranial sclerosis: non-random X-inactivation suggestive of X-linked dominant inheritance". Am J Med Genet A. Jun 15 2003;119A(3):400.

54. Vreeburg M, van Geel M, van den Heuij LG, Steijlen PM, van Steensel MA. Focal dermal hypoplasia in a male patient due to mosaicism for a novel PORCN single nucleotide deletion. J Eur Acad Dermatol Venereol. May 2011;25(5):592-5.
55. Monroe DG, McGee-Lawrence ME, Oursler MJ, Westendorf JJ. Update on Wnt signaling in bone cell biology and bone disease. Gene. Jan 15 2012;492(1):1-18.
56. Crockett JC, Rogers MJ, Coxon FP, Hocking LJ, Helfrich MH. Bone remodelling at a glance. J Cell Sci. Apr 01 2011;124(Pt 7):991-8.
57. Glatt V, Canalis E, Stadmeyer L, Bouxsein ML. Age-related changes in trabecular architecture differ in female and male C57BL/6J mice. J Bone Miner Res. Aug 2007;22(8):1197-207.
58. Syberg S, Petersen S, Beck Jensen JE, Gartland A, Teilmann J, Chessell I, et al. Genetic Background Strongly Influences the Bone Phenotype of P2X7 Receptor Knockout Mice. J Osteoporos. 2012;2012:391097.
59. Vanhoutteghem A, Maciejewski-Duval A, Bouche C, Delhomme B, Herve F, Daubigney F, et al. Basonuclin 2 has a function in the multiplication of embryonic craniofacial mesenchymal cells and is orthologous to disco proteins. Proc Natl Acad Sci U S A. Aug 25 2009;106(34):14432-7.

Figure 1: Design and molecular characterization of a *Wtx* allele.

A) Schematic drawing of the targeting strategy. White and black boxes signify coding (CDS) and untranslated (UTR) regions respectively. The domains previously described to be required for the interaction of WTX with APC (dashed boxes, APC1, APC4, APC2, APC3), Axin2 (conductin), WT1, β-catenin via the REA repeats, phosphatidyl inositol diphosphate (PIP2) and the region required for the nuclear localization are shown [7-9,11,12]. For the generation of the $Wtx^{flox\Delta}$ allele, loxP sites were inserted into intron 1 and within the coding region of exon2 (nucleotide position 1674). This results in the production of a shorter protein of 558 aminoacids due to the presence of two stop codons. Recombination between the loxP sites by Cre recombinase leads to a Wtx^{KO} allele where no functional protein is produced.

B) Immunostaining of HEK293 transfected cells reveals that wildtype GFP-WTX is found at the plasma membrane, within the cytoplasm and in 16% of cells in a speckled pattern within the nucleus. The shorter $\text{GFP-WTX}^{\text{flox}\Delta}$ protein maintained staining at the plasma membrane and the cytoplasm, but showed a much-reduced nuclear localization (4%). **Quantification** was done on three independent transfection experiments (n≥85 cells). Scale bar 10μm.

C) Co-transfection experiments followed by Co-IP analysis reveal that in contrast to GFP-WTX, $\text{GFP-WTX}^{\text{flox}\Delta}$ is no longer able to interact efficiently with WT1+KTS and WT1-KTS.

D) GFP-WTX, but not $\text{GFP-WTX}^{\text{flox}\Delta}$ is able to co-immunoprecipitate with β-catenin.

Numbers on the left of the images in **C, D** indicate positions of molecular weight markers (kD).

Figure 2. Characterization of $Wtx^{flox\Delta}$ and Wtx^{KO} alleles at birth.

A) X-ray analysis of postnatal day 0 (P0) pups demonstrates a rounder shape of the skull and bigger size of Wtx^{KO} neonates.

B) Frequency of perinatal death on the indicated genotypes.

C) Ventral view of dissected newborn heads show a full cleft of the secondary palate in 43% of Wtx^{KO} embryos (n=16).

D) Alizarin red/Alcian blue stained skeletal preparations at P0. Top view of the skull reveals wide cranial fontanelles (asterisk) and increased width (W) to length (L) ratio in Wtx^{KO} embryos. $Wtx^{flox\Delta}$ embryos show less marked altered cranial proportions.

E) Scatter plot showing the distribution (and mean) of the measurements in D). Mann-Whitney test: **p < 0.01; ***p < 0.001; ns, nonsignificant.

F) Inferior views of skull base after removal of the mandible. Two different Wtx^{KO} embryos are included to show variability of the phenotype (F', F''). Anterior view shows lack of fusion between the palatal processes of the maxillary and premaxillary bones (black arrowheads in F'). In cases of complete cleft of the secondary palate (F''), the palatal processes of the maxillary and palatine bones are severely hypoplastic or absent thus exposing the vomer and presphenoid. Small vertical arrows highlight convergence or not of the palatal processes of the palatine at the midline.

Posterior view shows the presence of a thin bony bridge between the basisphenoid and basioccipitale bone in 30% of $Wtx^{flox\Delta}$ embryos (white arrowhead**).** A thicker bridge (black arrowhead) and a hole in the basisphenoid bone or through the bridge (asterisks in F', F'') were present in 100% of Wtx^{ko} embryos (see Suppl. Table 1). bs=basisphenoid, bo=basioccipitale, ps=presphenoid, v=vomer, ppi=palatal process of premaxillary/incisive bone, ppm=palatal process of maxillary bone, ppp=palatal process of palatine.

G) Schematic representations of a control and complete cleft palate situation. The bone processes that fail to grow medially and anterior-posteriorly (arrows) to converge at the midline in the full cleft condition are outlined in blue. Adapted from [59].

n value ≥10 for all genotypes. Scale bars: D, 1000μm; F, 500μm

Figure 3. Skeletal abnormalities of $Wtx^{flox\Delta}$ and Wtx^{KO} alleles at birth.

Alizarin red/alcian blue stained skeletal preparations at postnatal day 0 (P0) reveal skeletal patterning and fusion defects in Wtx^{KO} embryos.

A) Reduction or absence of the deltoid tuberosity (dt, black arrowhead) and thickened radius (white arrowhead) in Wtx^{KO} embryos.

B) Occasional lack of fusion of lumbar vertebral bodies along the midline (asterisk) in Wtx^{KO} embryos. Vertebral bodies are often misshapen in the mutant (black arrowheads). Two different Wtx^{KO} embryos are shown to highlight variability of the phenotype.

C) Aberrant fusion of mutant sternebrae and xiphoid process leading to bifid sterna (black arrowheads). An asterisk in the anterior sternum depicts the presence of a stripe of cartilage in between the sternal bars of Wtx^{KO} embryos. In $Wtx^{flox\Delta}$ embryos fusion in the lower part of the sternum is often delayed (white arrowhead). Two different Wtx^{KO} embryos are shown to highlight variability of the phenotype. m=manubrium, s1-s4=sternebrae, xp=xiphoid process.

D) Scatter plot showing the distribution (and mean) of individual sternal measurements. Total length refers to the distance between the uppermost ossified part of the manubrium and the lowermost ossified part of the xiphoid process. Length of manubrium refers to the length of the ossified part and distance s1-s4 refers to the distance between the uppermost part of the ossification center s1 to the lowermost part of the ossification center s4 (Mann-Whitney test: ***$p < 0.001$; ns, nonsignificant). L3-L6=lumbar vertebrae, S1=sacral vertebrae.

n value ≥10 for all genotypes. Scale bars: A, 1000μm; B,C, 500μm

Figure 4: WTX$^{flox\Delta}$ interacts indirectly with β-catenin.

A) WTX$^{flox\Delta}$ interacts with coexpressed AXIN2 in HEK293 cells. Endogenous β-catenin and GSK3β also co-immunoprecipitate with WTX$^{flox\Delta}$ in the presence of AXIN2.

B) WTX$^{flox\Delta}$ recruits AXIN2 from the cytoplasm to the plasma membrane. Co-transfection of GFP-WTX or GFP-WTX$^{flox\Delta}$ (left panels, GFP fluorescence) together with Flag-AXIN2 (right panels, anti-Flag immunofluorescence) in MCF-7 cells.

C) WTX$^{flox\Delta}$ recruits GSK3 β from its diffuse cytoplasmic localization to the plasma membrane when AXIN2 is present. MCF-7 cells were cotransfected as indicated above the panels. GFP, GFP-WTX and GFP-WTX$^{flox\Delta}$ were detected by GFP fluorescence (left panels) and GSK3 β by anti-GSK3 β immunofluorescence (right panels).

D) MCF-7 cells were cotransfected as indicated below the bars. Quantification of the percentage of transfected GFP+ cells showing membrane localization of AXIN1, AXIN2 or GSK3β. Results are from one experiment scoring at least 20 cells using the 40x objective, and are representative of three independent experiments with similar phenotypes.

Figure 5. Elevated BMD in *Wtx* Mutant Mice

A-B) Radiographs from adult skulls showing altered skull proportions in female and male *Wtx* mutant mice.

C) Quantitation of skull morphometry from measurements on radiographs (see also Suppl. Figure 5A)

D) Scatter plot showing the distribution (and mean) of volumetric BMD (vBMD) of adult female and male WTX mutants.

E) Micro-CT analysis of femurs. BV/TV: bone volume/tissue volume, Ct.Th: cortical thickness, Tb.Th: trabecular thickness, Tb.Sp: trabecular separation, Tb.N, trabecular number, SMI: Structure model index. Whiskers represent the 5th and the 95th percentile.

n value ≥7 for all genotypes. Student t-test: *p <0.05; **p < 0.01; ***p < 0.001.

Comai et al.,
Figure 1

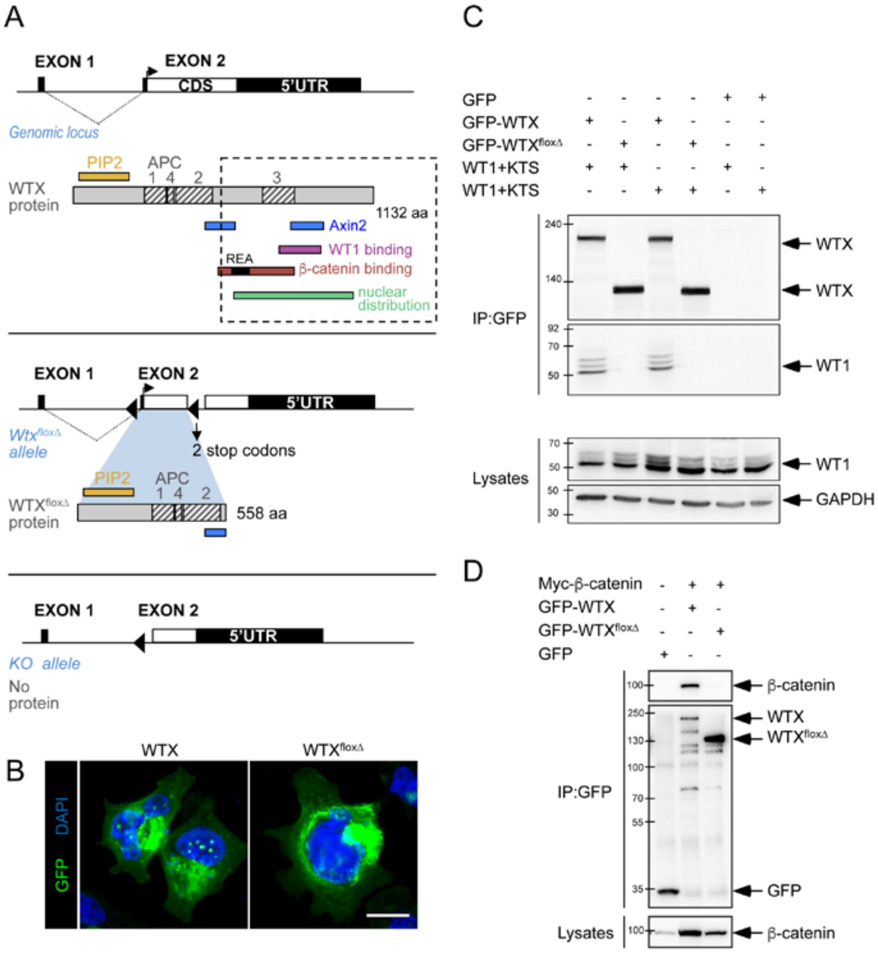

Comai et al.,
Figure 2

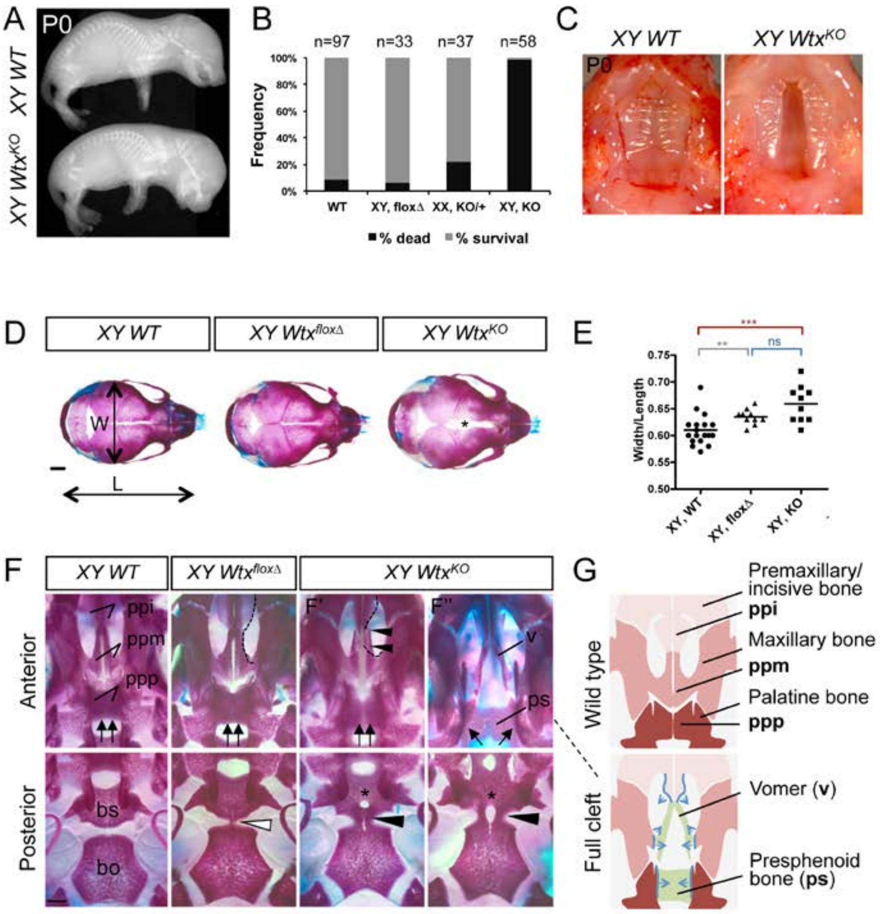

Comai et al.,
Figure 3

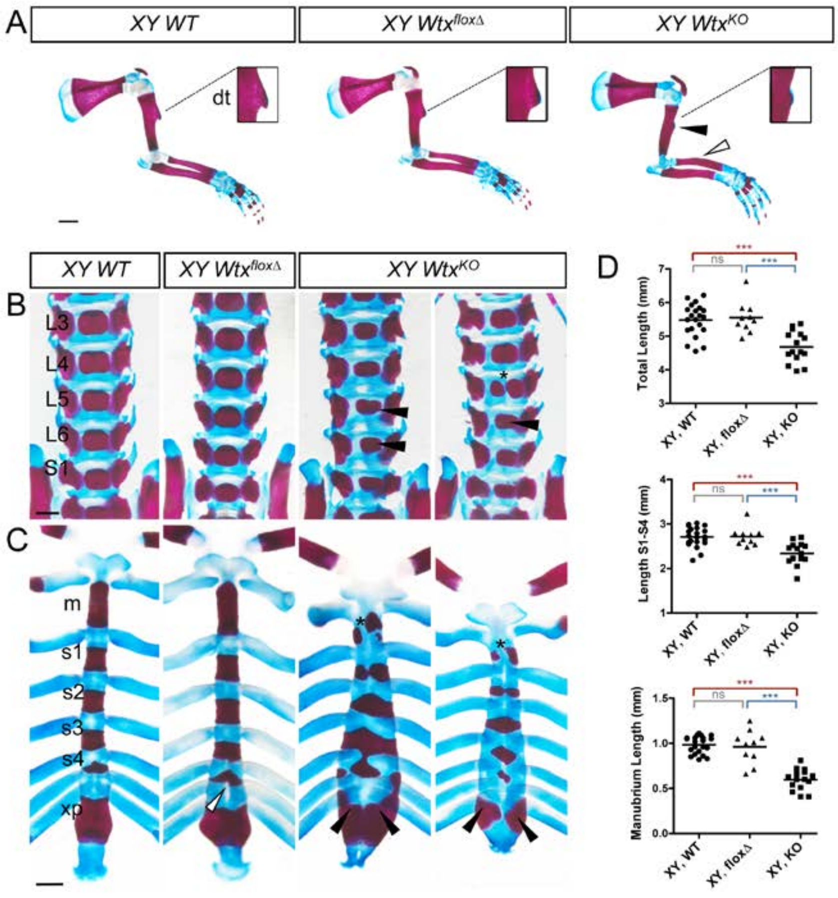

Comai et al.,
Figure 4

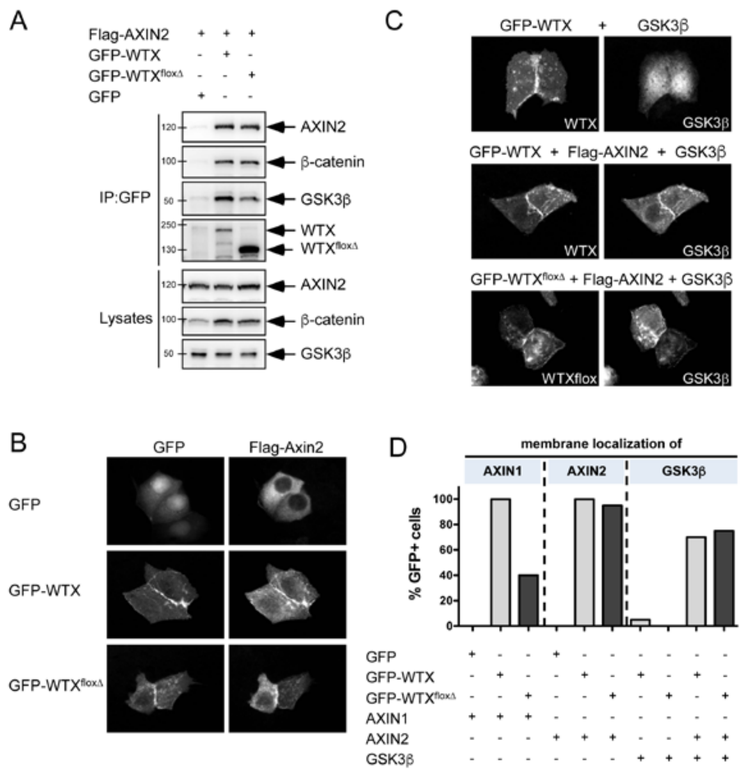

Comai et al.,
Figure 5